High T_1- and T_2-Contrast Ability of Ultra-Fine PEGylated Iron Oxide Nanoparticles in Ultra-Low Field MRI Measured By a High-T_c DC-SQUID

Jin Yirong, Jia Qiaojuan, Deng Hui, Wang Ning, Jiang Fengying, Tian Ye, Gao Mingyuan, and Zheng Dongning

Abstract*—The effect of ultra-fine superparamagnetic PEGylated iron oxide nanoparticles (SPIONs) on the ^{1}H nuclei spin relaxation time T_1 and T_2 were systematically investigated for the performance as T_1 or T_2 contrast agents in ultra-low field (ULF) nuclear magnetic resonance and resonance imaging (NMR&MRI). A high-T_c dc-SQUID sensor was used to detect the resonance signal from water samples containing SPIONs of different sizes and concentrations. The relaxation rates ($T_{1,2}^{-1}$) was shown to depend linearly on the iron concentration (C, in mMol of Fe). The relaxivities (defined as $d(T_{1,2}^{-1})/dC$) r_1 and r_2 were fitted and compared with high field (3 T) NMR results. An impressive improvement of more than an order in r_1 was found for all SPIONs of different sizes, which leads to a much lowered relaxivity ratio r_2/r_1. For all SPIONs measured, r_2/r_1 was around 1, which implies that SPIONs are high performance T_1 contrast agent in ULF NMR&MRI. The highest r_1 and r_2 values were found in the sample containing 16.7 nm nanoparticles, both of them being around 200 $\mathrm{mMol}^{-1}\mathrm{s}^{-1}$. Furthermore, we also demonstrated T_1-weighted contrast imaging using 16.7 nm nanoparticles. Clear intensity gradient were shown in the images, indicating a good contrast enhancement capability.

***Index Terms*—Contrast agent, MRI, SQUID, superparamagnetic iron oxide nanoparticles, ultra-low field NMR.**

I. INTRODUCTION

ULTRA LOW FIELD (ULF) nuclear magnetic resonance (NMR) has attracted considerable interests since the introduction of superconducting quantum interference device (SQUID) as the sensor of the resonance signal [1]–[4]. When combined with pre-polarization [4], the signal-to-noise ratio (SNR) of ULF-NMR can be greatly improved, reaching the requirement for magnetic resonance imaging (MRI). Due to its advantages in spectroscopy (narrow spectrum linewidth, negligible chemical shift) and imaging (negligible susceptibility artifact, enhanced T_1 contrast, insusceptible to metallic objects) [5]–[7], in addition with its low-cost nature, ULF-NMR was considered as a prospective supplement to high field NMR technologies. After decades of development, fruitful results were obtained and many kinds of measurement configuration were proposed [8]–[15]. ULF-MRI for parts of human body or other bio-samples were also realized by different groups [16]–[21].

MRI is a very powerful tool for biological molecular imaging and clinical diagnosis. Three dimensional tomographic information can be acquired by MRI with high spatial resolution without the use of radiation or radiotracers. By applying different pulse sequences to control the polarization and re-focus of nuclear spins, T_1 or T_2 weighted MRI can be obtained with higher contrast between normal and pathological tissues [22]. In many cases, an even higher contrast is required to ensure precise diagnosis in earlier stage of diseases, resulting in the development of exogenous contrast agents [23], [24].

Superparamagnetic PEGylated iron oxide nanoparticles (SPIONs) are one class of contrast agents commercially available in high-field MRI [25]. These nanoparticles generally act as T_2 contrast agent because of their high relaxivity ratio, r_2/r_1, which is commonly larger than 10 [26]. Since T_2 weighted imaging is negative contrast enhancement where tissues with high agent concentration will appear dark, it has low specificity in distinguish diseased tissues, because the signal is often confused with that from bleeding, calcification or other tissues having similar T_2 values [26], [27]. This negative contrast effect, along with the susceptibility artifact problem, become the main restricts for the applications of SPIONs in high field MRI.

In this work, we studied the behavior of longitudinal (T_1^{-1}) and transverse relaxation rate (T_2^{-1}) of ^{1}H spins in water samples containing different concentration of SPIONs in a home-build ULF-NMR & MRI system measured by a high-T_c dc-SQUID sensor. The results show very high T_2 relaxivities r_2,

---

Manuscript received August 12, 2014; accepted October 1, 2014. Date of publication October 17, 2014; date of current version December 15, 2014. This work was supported in part by the National Basic Research Program of China (973 Program, No. 2011CBA00106 and No. 2011CB935800), National Natural Science Foundation of China under Grant 11104333, and Strategic Priority Research Program of the Chinese Academy of Sciences under Grant XDB07000000.

J. Yirong, D. Hui, J. Fengying, T. Ye, and Z. Dongning are with the Beijing National Laboratory for Condensed Matter Physics, Institute of Physics, Chinese Academy of Sciences, Beijing 100190, China (e-mail: jyr-king@iphy.ac.cn).

J. Qiaojuan was with the Institute of Chemistry, Chinese Academy of Sciences, Beijing 100190, China. She is now with the School of Chemistry and Environment, South China Normal University, Guangzhou 510006, China (e-mail: jiaqj@iccas.ac.cn).

W. Ning was with the Beijing National Laboratory for Condensed Matter Physics, Institute of Physics, Chinese Academy of Sciences, Beijing 100190, China. He is now with the High Magnetic Field Laboratory, Chinese Academy of Sciences, Hefei 230031, China (e-mail: wn127@126.com).

G. Mingyuan is with the Institute of Chemistry, Chinese Academy of Sciences, Beijing 100190, China (e-mail: gaomy@iccas.ac.cn).

Color versions of one or more of the figures in this paper are available online at http://ieeexplore.ieee.org.

Digital Object Identifier 10.1109/TASC.2014.2363630

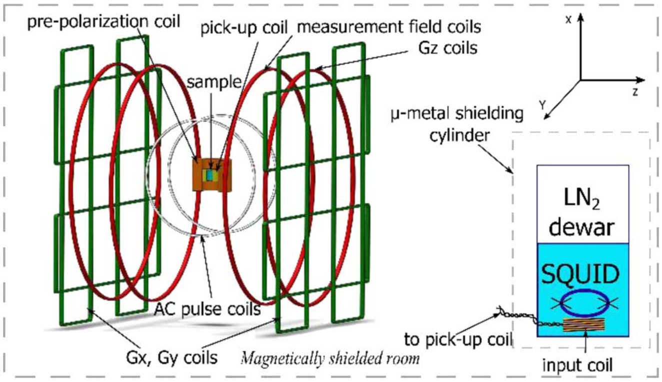

Fig. 1. A schematic of our ULF-NMR coil system. A high-T$_c$ dc-SQUID and input coil were immersed into the bottom of a LN$_2$ Dewar (lower right), which was then further protected by a 3-layer μ-metal shielding cylinder. On the top right corner is the reference coordinates we used in this work.

close to that measured under high field (3 T). Furthermore, the T_1 relaxivities r_1 were found to be more than an order higher than that under high field, resulting the relaxivity ratio r_2/r_1 close to or even less than 1. This indicates that SPIONs in ULF-NMR can act as very high performance T_1 or $T_1 - T_2$ dual contrast agents. In addition with the negligible susceptibility artifacts in ULF MR imaging, SPIONs may find their wide range applications in ULF NMR & MRI technology, for example, the early diagnosis of prostate cancer, breast cancer, and so on.

II. EXPERIMENTAL

A. *Synthesis of* $\mathrm{Fe_3O_4}$ *Nanocrystals*

Different sized $\mathrm{Fe_3O_4}$ nanocrystals were prepared according to the method described in the literature [28]. Typically, 2.12 g (6 mMol) of $\mathrm{Fe(acac)_3}$, 7.90 mL (24 mMol) of oleylamine and 24.0 g (12 mMol) of HOOC-PEG-COOH were dissolved in 100 mL diphenyl oxide solution, and the stock solution was obtained after being purged with nitrogen for 2 h. The stock solutions were aged at different temperatures for several hours to obtain different sized $\mathrm{Fe_3O_4}$ nanocrystals followed by heating the stock solutions to reflux for 30 min. The nanocrystals were collected by dispersed in ethanol and subsequently precipitated with ether.

The as-prepared $\mathrm{Fe_3O_4}$ nanocrystals show good colloid stability in water and physiological system as PEG is a typical excellent biocompatible polymer.

B. *ULF-NMR & MRI System*

Our ULF-NMR & MRI system was built inside a home-made magnetically shielded room (MSR). Residual field in the center of the MSR was measured to about 170 nT. Nuclear spins are firstly pre-polarized by a solenoid coil which can generate a field of ~16 mT/A (along x direction, the axes are shown in Fig. 1). A measurement field of about 67 μT is constantly applied by a pair of Helmholtz coils with diameter 60 cm (in z direction). After polarized for a few seconds (usually 1–8 sec., depends on the T_1 value of the sample), the pre-polarization field turns off nonadiabatically and then the nuclear spins start to do Larmor precession. A solenoid pick-up coil fitted between the pre-polarization coil and the sample space inductively couples the free induction decay (FID) signal and transfer the signal to an input coil mounted beneath a high-T$_c$ dc-SQUID. The SQUID sensor used in this study was supplied by Forschungszentrum Jülich in Germany [29]. The field sensitivity in the white noise range is about 30 $\mathrm{fT/Hz^{1/2}}$ (1/f noise corner is at about 20 Hz) when measured in a well shielded space. However, it degraded to about 100 $\mathrm{fT/Hz^{1/2}}$ because of environmental field fluctuation or trapped flux in the pick-up loop of the SQUID [30]. The pick-up and input coils were carefully designed and wound with resistances and inductances of 2.2 Ω and 6.3 mH, 3.2 Ω (at liquid nitrogen temperature) and 27 μH, respectively [21]. The Johnson noise current in the loop can be estimated to about 0.1 $\mathrm{nA/Hz^{1/2}}$, which will give an additional flux noise on the order of the sensor's noise (1/f noise corner is at about 200 Hz). A switch and a specified capacitance are connected in series of the loop, forming a tank circuit so that the coupling around the resonance frequency will be enhanced. In addition, the input coil and SQUID are placed at the bottom of a glass-fiber Dewar surrounded by a 3-layer μ-metal magnetically shielded cylinder. Such a configuration can obtain much higher coupling efficiency compared to directly coupling to the SQUID sensor, while avoid the influence from the strong pre-polarization field to the SQUID. Gradient field coils (a pair of Maxwell coils to generate $\partial B_\mathrm{m}/\partial z$, two set of bi-planar coils to generate $\partial B_\mathrm{m}/\partial x$ and $\partial B_\mathrm{m}/\partial y$) were also designed and installed for imaging experiments, and a pair of Helmholtz coils (along y axis, diameter 24 cm) is used to generate pulsed AC field. A schematic of the whole ULF-NMR & MRI system is shown in Fig. 1. More details about the system configuration and performance were described in the literatures [15], [21], [31]. Typical signal-to-noise ratio for single-shot FID measurement of water sample with a volume of ~15 mL was obtained to be over 200 (Fig. 2).

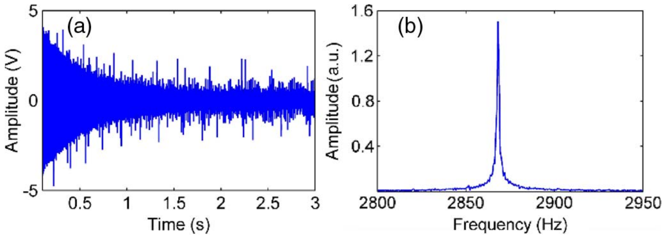

Fig. 2. A typical single-shot measurement result of FID in ~15 mL water. The SNR was estimated to ~220. The measurement conditions were as follow: $B_\mathrm{m} \sim 67\ \mu\mathrm{T}$, $B_\mathrm{p} \sim 34\ \mathrm{mT}$, $T_\mathrm{p} = 6\ \mathrm{sec}$.

C. *Sample Preparation*

Water samples with different Fe concentrations were prepared in a clean room. Four kinds of stock solutions with different average particle sizes were used: 10.3 nm, 12.0 nm, 14.1 nm and 16.7 nm. The concentrations are 3.5 mg/mL, 3.16 mg/mL, 2.26 mg/mL and 3.63 mg/mL, respectively (it should be noticed that these values are the mass concentrations of Fe, not $\mathrm{Fe_3O_4}$). Preparation of 16.7 nm nanoparticle solutions is demonstrated here: 60 μL stock solution was transferred into a 25 mL

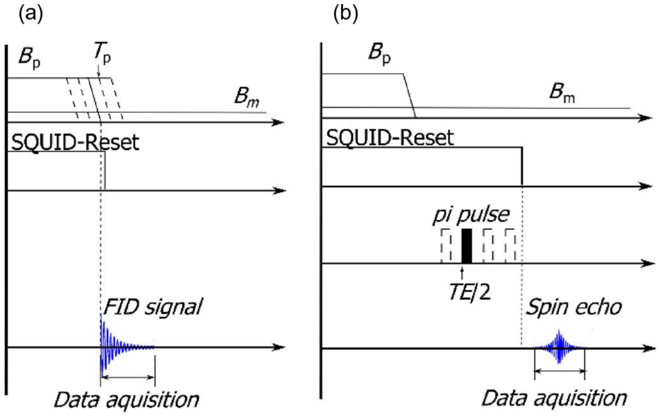

Fig. 3. (a) Pulse-sequence for T_1 measurement. T_p correspond to pre-polarization time. (b) Pulse sequence for T_2 measurement. $TE/2$ corresponds to the time interval between the start of FID and the π-pulse.

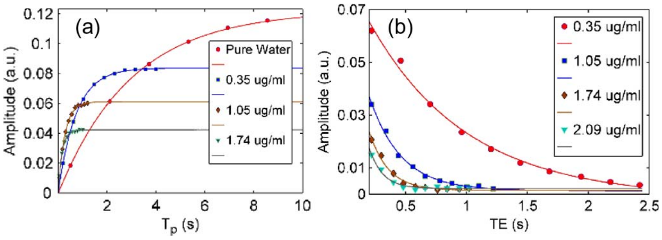

Fig. 4. (a) FID amplitudes vs. pre-polarization time T_p for different Fe (16.7 nm) concentrations. (b) Spin-echo amplitudes vs. echo time TE for different Fe (16.7 nm) concentrations.

volumetric flask by a pipette, then dilute to volume by deionized water and mix. After that, volumes of 1, 2, 3, 4, 5, and 6 mL diluted solution were transferred into six dry volumetric flasks (also 25 mL) respectively, using appropriate pipettes. The final step was dilute to volume for all the six flasks, fully mix and then transfer into small bottles with volumes of about 15 mL. As a result, the final concentrations were 0.35 $\mu\mathrm{g/mL}$, 0.70 $\mu\mathrm{g/mL}$, 1.05 $\mu\mathrm{g/mL}$, 1.39 $\mu\mathrm{g/mL}$, 1.74 $\mu\mathrm{g/mL}$ and 2.09 $\mu\mathrm{g/mL}$. Solutions for other particle sizes were prepared by the same way. Their final concentrations were controlled to nearly in the same range as 16.7 nm solutions.

D. T_1 and T_2 Measurements

T_1 was obtained by measuring the FID amplitude after different pre-polarization time, and then fitted by the following equation:

$$S = S_0\left[1 - \exp\left(\frac{-t}{T_1}\right)\right].$$

T_2 was obtained by measuring the spin echo amplitude with π-pulses applied at different delay time. A small gradient field (~80 nT/cm) was also applied during the measurement to suppress the FID. Time sequences for T_1 and T_2 measurements are shown in Fig. 3. Fig. 4 gives some typical measured results of T_1 and T_2 relaxations. It is easy to see that with the iron concentration increases, both T_1 and T_2 become more and more short.

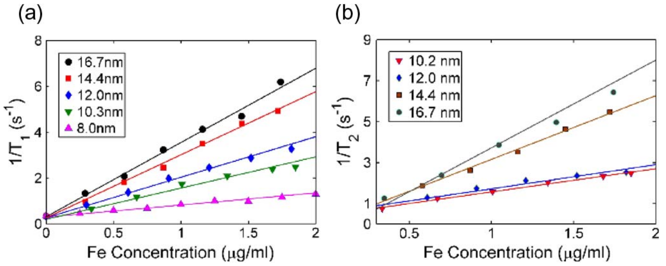

Fig. 5. (a) T_1^{-1} vs. Fe concentration for different SPION sizes. (b) T_2^{-1} vs. Fe concentration for different SPION sizes. The solid lines are linear fittings to the measurement results.

TABLE I

T_1 AND T_2 RELAXIVITIES FOR SPIONS WITH DIFFERENT SIZES

Sizes (nm)	r_1 (mM^{-1}s^{-1}) 67 µT	3 T	r_2 (mM^{-1}s^{-1}) 67 µT	3 T	r_2/r_1 67 µT	3 T
10.3	68.5	4.4	61.0	105.6	0.89	24.0
12.0	92.2	4.5	66.1	198.4	0.72	44.1
14.1	155.2	2.8	163.5	191.0	1.05	68.2
16.7	188.3	2.8	220.6	231.1	1.17	82.5

III. RESULTS AND DISCUSSION

After T_1 and T_2 relaxation time were fitted out for the samples of different SPION sizes and concentrations, we plot them together, as shown in Fig. 5. The relaxation rates (T_1^{-1} and T_2^{-1}) increase almost linearly with increasing the SPION concentration C. Such results are in accordance with high field NMR results. Linear fitting to those curves can give some important parameters for applications as contrast agents, those are: Relaxivity $r_1(d(T_1^{-1})/dC)$, relaxivity $r_2(d(T_2^{-1})/dC)$ and their ratio r_2/r_1. For the application of SPIONs as contrast agent, high relaxivities are always preferred, because it indicates that less quantity of the agents will be needed to get an image with the required contrast. r_2/r_1 determines which kind of contrast agent it is suitable for. To act as T_1 contrast agent, r_2/r_1 ratio cannot be too large, it is generally required to be close to 1. For larger r_2/r_1 ratio, they can only be used as T_2 contrast agent.

As a comparison, r_1 and r_2 data were also measured by a commercial MRI system (GE signa 3.0 T HD, Milwaukee, WI). In Table I, we list all the r_1 and r_2 data measured in this study and in high field for different SPION sizes. From the table, we can see that under low field, both r_1 and r_2 increase when the particle size is increased. Under high field, r_2 also has such a trend, but r_1 decreases a little for larger sizes (14.1 and 16.7 nm).

Another important information is that, r_1 under ultra-low field is much higher than that under high field. This results in much lower r_2/r_1 ratio. For all the samples measured in this study, the r_2/r_1 ratio value is very close to 1, or even less than 1 for smaller particle sizes (10.3 and 12.0 nm). As the criteria stated above, it means that our SPIONs can act as T_1 contrast agents. Furthermore, it is remarkable to notice that r_1 value for 16.7 nm SPIONs is nearly 200 $\mathrm{mM^{-1}s^{-1}}$, which is more than 60 times larger than the value of typical T_1 contrast agent magnevist (Gd-DTPA, 3.6 $\mathrm{mM^{-1}s^{-1}}$, 1.5 T) [31]. Still its r_2/r_1 value is nearly 1. As a result, it is convincing that SPIONs can

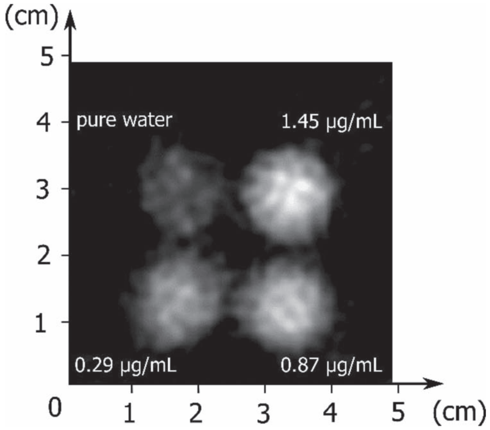

Fig. 6. A typical T_1-contrast image obtained by filtered back-projection method. Four tubes with different iron concentrations (indicated in the figure) of 16.7 nm nanoparticles were arranged together to demonstrate the contrast enhancement.

be very high performance T_1 contrast agents under low-field. In the same time, their high r_2 values make them also high performance T_2 contrast agents. Iron oxide nanoparticles were also studied in high field MRI as T_1 contrast agents, but the r_1 values are still far smaller than our results, and r_2/r_1 values are also larger than 1, close to 2 [26], [32], [33].

To demonstrate the T_1-contrast capability of SPIONs in ULF-NMR/MRI, we performed 2D MRI on water samples with different concentration of 16.7 nm SPIONs. A filtered back-projection method was used to reconstruct 2D MR images. A typical imaging result is shown in Fig. 6. 24 projection angles were chosen. For each angle, the signal was averaged for 20 times. The pre-polarization time T_p was chosen to 0.5 sec., and the echo time TE was set to 0.3 sec. From the image, we can see that as the concentration of SPIONs increases, the signal density also increase significantly, shown good contrast enhancement.

IV. CONCLUSION

In summary, we have studied the influence of SPIONs to the relaxation rates of ^{1}H nuclei spins in water samples by a home-built ULF-NMR & MRI system. SPIONs with different sizes from 10.3–16.7 nm were used in the study. The measured relaxation rates show linear increasing with increasing of the Fe concentration. T_1 and T_2 ralaxavities (r_1 and r_2) were deduced from such linear relationship and compared to that obtained under a commercial 3 T MRI system. For larger particle sizes (14.1 and 16.7 nm), the r_2 values are close to the high field results, showing good T_2-contrast capability. In addition, they also show very high r_1 that is more than 60 times larger than standard T_1-contrast agent based on Gd^{3+} chelate in high field MRI. The relaxavity ratios r_2/r_1 are closed to 1, indicating that these SPIONs can act as high performance T_1-contrast agents in ULF-MRI.

REFERENCES

[1] L. J. Friedman, A. K. M. Wennberg, S. N. Ytterboe, and H. M. Bozler, “Direct detection of low-frequency NMR using a dc SQUID,” *Rev. Sci. Instrum.*, vol. 57, no. 3, pp. 410–413, Mar. 1986.

[2] C. Connor, J. Chang, and A. Pines, “Magnetic resonance spectrometer with a dc SQUID detector,” *Rev. Sci. Instrum.*, vol. 61, no. 3, pp. 1059–1063, Mar. 1990.

[3] S. Kumar, W. F. Avrin, and B. R. Whitecotton, “NMR of room temperature samples with a flux-locked dc SQUID,” *IEEE Trans. Magn.*, vol. 32, no. 6, pp. 5261–5264, Nov. 1996.

[4] A. I. Braginski, *The SQUID Handbook: Fundamentals and Technology of SQUIDs and SQUID Systems*, 1st ed. Weinheim, Germany: Wiley-VCH, 2004.

[5] J. Clarke, M. Hatridge, and M. Mössle, “SQUID-detected magnetic resonance imaging in microtesla fields,” *Annu. Rev. Biomed. Eng.*, vol. 9, pp. 389–413, 2007.

[6] J. Bernarding *et al.*, “J-Coupling nuclear magnetic resonance spectroscopy of liquids in nT fields,” *J. Amer. Chemical Soc.*, vol. 128, no. 3, pp. 714–715, Jan. 2006.

[7] M. Mößle *et al.*, “SQUID-detected microtesla MRI in the presence of metal,” *J. Magn. Resonance*, vol. 179, no. 1, pp. 146–151, Mar. 2006.

[8] M. Mossle *et al.*, “SQUID-detected in *vivo* MRI at microtesla magnetic fields,” *IEEE Trans. Appl. Supercond.*, vol. 15, no. 2, pp. 757–760, Jun. 2005.

[9] L. Qiu, Y. Zhang, H.-J. Krause, A. I. Braginski, and A. Usoskin, “High-temperature superconducting quantum interference device with cooled LC resonant circuit for measuring alternating magnetic fields with improved signal-to-noise ratio,” *Rev. Sci. Instrum.*, vol. 78, no. 5, May 2007, Art. ID. 054701.

[10] L. Q. Qiu *et al.*, “High-performance low-field NMR utilizing a high-T$_\mathrm{c}$ rf SQUID,” *IEEE Trans. Appl. Supercond.*, vol. 19, no. 3, pp. 831–834, Jun. 2009.

[11] C. Liu *et al.*, “Permanent magnet pre-polarization in low field MRI measurements using SQUID,” *Phys. Procedia*, vol. 36, pp. 274–279, 2012.

[12] H.-C. Yang *et al.*, “Enhancement of nuclear magnetic resonance in microtesla magnetic field with prepolarization field detected with high-T$_\mathrm{c}$ superconducting quantum interference device,” *Appl. Phys. Lett.*, vol. 88, no. 25, Jun. 2006, Art. ID. 252505.

[13] S.-H. Liao *et al.*, “Sensitive J-coupling spectroscopy using high-T$_\mathrm{c}$ superconducting quantum interference devices in magnetic fields as low as microteslas,” *Supercond. Sci. Technol.*, vol. 22, no. 4, Apr. 2009, Art. ID. 045008.

[14] K.-L. Chen *et al.*, “A signal input coil made of superconducting thin film for improved signal-to-noise ratio in a high-T$_\mathrm{c}$ SQUID-based ultra-low field nuclear magnetic resonance system,” *Supercond. Sci. Technol.*, vol. 26, no. 11, Nov. 2013, Art. ID. 115008.

[15] N. Wang *et al.*, “Detection of nuclear magnetic resonance in the microtesla range using a high T$_\mathrm{c}$ dc-SQUID,” *J. Phys.: Conf. Ser.*, vol. 400, no. 5, Dec. 2012, Art. ID. 052041.

[16] V. S. Zotev *et al.*, “Microtesla MRI of the human brain combined with MEG,” *J. Magn. Resonance*, vol. 194, no. 1, pp. 115–120, 2008.

[17] V. S. Zotev *et al.*, “Parallel MRI at microtesla fields,” *J. Magn. Resonance*, vol. 192, no. 2, pp. 197–208, Jun. 2008.

[18] B. Inglis *et al.*, “MRI of the human brain at 130 microtesla,” in *PNAS*, Nov. 2013, vol. 110, no. 48, pp. 19194–19201.

[19] C. Liu *et al.*, “Tuned HTS SQUID-detected low field MRI using a permanent magnet for pre-polarization with automatic transportation,” *IEEE Trans. Appl. Supercond.*, vol. 23, no. 3, Jun. 2013, Art. ID. 1601104.

[20] S. H. Liao *et al.*, “Microtesla NMR and High Resolution MR imaging using high—SQUIDs,” *IEEE Trans. Appl. Supercond.*, vol. 23, no. 3, Jun. 2013, Art. ID. 1602404.

[21] N. Wang *et al.*, “Ultra-low field magnetic resonance imaging based on high T$_\mathrm{c}$ dc-SQUID,” *Acta Phys. Sin.*, vol. 61, no. 21, 2012, Art. ID. 213302.

[22] D. D. Stark, *Magnetic Resonance Imaging*, 3rd. St. Louis, MO, USA: C.V. Mosby, 1999.

[23] H. H. Chen *et al.*, “Relaxation rates of protons in gadolinium chelates detected with a high-T$_\mathrm{c}$ superconducting quantum interference device in microtesla magnetic fields,” *J. Appl. Phys.*, vol. 108, no. 9, Nov. 2010, Art. ID. 093904.

[24] H. C. Yang *et al.*, “Relaxation of biofunctionalized magnetic nanoparticles in ultra-low magnetic fields,” *J. Appl. Phys.*, vol. 113, no. 4, Jan. 2013, Art. ID. 043911.

[25] Y. Xiang and J. Wang, “Superparamagnetic iron oxide based MRI contrast agents: Current status of clinical application,” *Quant Imaging Med Surg*, vol. 1, no. 1, pp. 35–40, Dec. 2011.

[26] F. Hu, Q. Jia, Y. Li, and M. Gao, “Facile synthesis of ultrasmall PEGylated iron oxide nanoparticles for dual-contrast T$_1$- and T$_2$-weighted magnetic resonance imaging,” *Nanotechnology*, vol. 22, no. 24, Jun. 2011, Art. ID. 245604.

[27] S. Busch *et al.*, “Measurements of T_1-relaxation in ex vivo prostate tissue at 132 $\mu\mathrm{T}$,” *Magn. Reson. Med.*, vol. 67, no. 4, pp. 1138–1145, Apr. 2012.

[28] Q. Jia *et al.*, “Gelification: An effective measure for achieving differently sized biocompatible $\mathrm{Fe_3O_4}$ nanocrystals through a single preparation recipe,” *J. Am. Chem. Soc.*, vol. 133, no. 48, pp. 19512–19523, Dec. 2011.

[29] [Online]. Available: http://www.fz-juelich.de/pgi/pgi-5/EN/Forschung/SensorikUndSpektrometrie/_node.html

[30] Y. R. Jin *et al.*, “The Effect of low frequency external field disturbance on the SQUID based ultra-low field NMR measurements,” *IEEE Trans. Appl. Supercond.*, vol. 21, no. 3, pp. 518–521, Jun. 2011.

[31] N. Wang *et al.*, “Ultra-low-field MRI and spin-lattice relaxation time of $^1\mathrm{H}$ in the presence of $\mathrm{Fe_3O_4}$ magnetic nano-particles detected with a high-T_C dc-SQUID,” *IEEE Trans. Appl. Supercond.*, vol. 23, no. 3, Jun. 2013, Art. ID. 1602504.

[32] U. I. Tromsdorf, O. T. Bruns, S. C. Salmen, U. Beisiegel, and H. Weller, “A highly effective, nontoxic T_1 MR contrast agent based on ultrasmall PEGylated iron oxide nanoparticles,” *Nano Lett.*, vol. 9, no. 12, pp. 4434–4440, Dec. 2009.

[33] S. Kenouche *et al.*, “NMR investigation of functionalized magnetic nanoparticles $\mathrm{Fe_3O_4}$ as $\mathrm{T}_1-\mathrm{T}_2$ contrast agents,” *Powder Technol.*, vol. 255, pp. 60–65, Mar. 2014.